

Simultaneous Determination of Ascorbic Acid, Dopamine and Uric Acid Based on Graphene/Polyaniline/Gold Nanohybrids

Ling Shi^{1,2}, Zefeng Wang^{1,2,*}, Gaozhang Gou^{1,2}, Xianlan Chen^{1,2}, Guangming Yang^{1,2}, Wei Liu^{1,2,*}

¹ School of science, Honghe University, Mengzi, Yunnan 661199, PR China

² Key Laboratory of Natural Pharmaceutical & Chemical Biology of Yunnan Province, Mengzi, Yunnan 661199, PR China

*E-mail: wangzefeng841006@163.com, liuwei4728@126.com

Received: 24 October 2016 / Accepted: 16 January 2017 / Published: 12 February 2017

A novel method for preparing graphene/polyaniline (GN/PANI) nanocomposites was demonstrated by liquid-liquid interface polymerization method. Then gold nanoparticles (Au NPs) were uniformly and controllably decorated on the surface of the GN/PANI to form graphene/polyaniline/gold (GN/PANI/Au) nanohybrids. The prepared nanocomposites were characterized by the UV-vis spectra, X-ray diffraction and transmission electron microscopy. The electrochemical sensor based on GN/PANI/Au nanohybrids was fabricated for the simultaneous detection of ascorbic acid (AA), dopamine (DA) and uric acid (UA). The results showed that three well-resolved oxidation peaks were observed in cyclic voltammetry (CV) and differential pulse voltammetry (DPV) measurements. And the corresponding DPV current signals have appeared as well resolved oxidation peaks with peak potential differences of 186 mV (AA-DA), 156 mV (DA-UA), and 342 mV (AA-UA).

Keywords: Graphene, Polyaniline, Gold nanoparticles, Dopamine, Ascorbic acid, Uric acid

1. INTRODUCTION

Ascorbic acid (AA), dopamine (DA), and uric acid (UA) are always coexisted in the extracellular fluid, which play a vital role in human metabolism. DA is a catecholamine neurotransmitter that plays a significant role in the human brain chemistry. Low levels of DA can cause brain disorders such as schizophrenia and Parkinson's disease [1]. AA is another requisite component in human life, it is especially important in bioelectrochemistry, neurochemistry, and clinical diagnostics applications. More importantly, it has been used to prevent and treat common cold, scurvy, hepatic disease, AIDS and cancer [2]. In human body UA is the primary end product of purine metabolism, and it is a significant biomolecule present in urine and serum. Extreme abnormalities of UA levels are associated with several diseases such as higher levels lead to hyperuricemia, gout and

Lesch-Nyhan syndrome [3, 4]. Therefore, it is of extremely importance to detect these species with desired sensitivity and accuracy. However, AA, DA and UA usually coexist in biological fluids and the electrochemical activity of these substances is very similar. Hence, the selective, rapid and simultaneous detection of AA, DA and UA is of urgent desired in medical diagnosis and biological analysis.

In recent years, by taking advantage of the unique properties of nanomaterials, the detection performance of electrochemical sensors has been largely improved. To date, a lot of novel nanostructured materials have been successfully utilized to construction of electrochemical sensing platforms for the sensitive detection of AA, DA and UA. Typical examples are NiCo₂O₄ nanowires functionalized graphene fibers [5], gold nanoclusters ensemble-on-activated graphene/MWCNT [6], reduced graphene oxide/zinc sulfide nanocomposite [7], etc. All these related studies indicated that sensing platforms fabricated from nanomaterials can significantly enhance detection performance for AA, DA and UA. Thus, it is highly desirable to design new nanomaterial to enhance the electrochemical properties of electrochemical sensors for sensitively and selectively detecting AA, DA and UA.

Graphene (GN) is an intriguing two-dimensional carbon material that carbon atoms densely packed in honey-comb crystal lattice. It has attracted much research attention, such as sensors [7], fuel cells [8], capacitors [9], etc., due to its high electrocatalytic activity and excellent conductivity [10]. Unfortunately, graphenes tend to adhere one another into graphitic sheets due to high van der Waals energy. Therefore, it is an urgent task for production a homogeneous colloidal suspension. Among conducting polymers family, polyaniline (PANI) has been the most extensively studied one with respect to its many advantages such as easy and straightforward preparation, low cost and high polymerization yield, unique electrochemical properties, relatively high conductivity, and most importantly its reversible (acid/base) doping/dedoping pathways identified with its structural chain nitrogen [11]. On the other hand, gold nanoparticles (Au NPs) are of considerable interest due to their merits of large specific surface area, good solubility, excellent conductivity and biocompatibility. Au NPs can greatly increasing the electron transfer between redox centers and electrode surfaces and can act as catalysts to increase the rate of electrochemical reactions [12].

In this work, we report a simple method for synthesizing stable aqueous dispersions of graphene/polyaniline (GN/PANI) composites utilized an interfacial polymerization approach. GN can considerably improve the stability of PANI and that PANI increases the dispersion ability of GN in aqueous solution. Then the prepared GN/PANI composites were used for the in situ preparation of Au NPs. The GN/PANI/Au nanohybrids were employed to investigate the effect of simultaneous determination of AA, DA and UA.

2. EXPERIMENTAL

2.1 Materials

Graphite flake (99.8%, 8000 mesh) was provided by aladdin. Hydrogen tetrachloroaurate (III) hydrate were purchased from the Shanghai sybridge Chemical Reagent Company. Ascorbic acid, dopamine and uric acid were purchased from Sigma-Aldrich. H₂SO₄, FeCl₃·6H₂O, NaBH₄, H₂O₂,

CH_2Cl_2 , and other reagents were of analytical grade and used without further purification. Aniline was fresh distillation prior to use. The phosphate buffer solution was prepared using NaH_2PO_4 and Na_2HPO_4 . All aqueous solutions were prepared with doubly distilled water.

2.2 Preparation of GN/PANI nanocomposites

Graphite oxide (GO) was synthesized from graphite flake by a modified Hummers method [13, 14]. Chemical conversion of graphite oxide to GN was carried out according to the reported method [15, 16], and the details were described in the literature [17]. GN/PANI nanocomposites were prepared by a modified method described in our previous paper [18], and the procedures are briefly described as follows. GN/PANI nanocomposites were synthesized using the liquid-liquid interfacial polymerization method. Typically interfacial reaction was performed in a 20 mL glass vial. Aniline (5 mg) was dissolved in CH_2Cl_2 (5 mL) and served as the lower organic layer. GNs (0.15 mg), H_2O_2 (26.5 μL) and $\text{FeCl}_3 \cdot 6\text{H}_2\text{O}$ (5 mg) were dispersed in HCl (5 mL, 1.0 M) aqueous solution by bath-sonicating for 1 h, and formed the upper layer. After the interfacial system was established, the resulting two-phase system was left undisturbed at an ice bath for 48 h. Polymerization can be observed when the characteristic green color of polyaniline emeraldine salt became visible. At the end of polymerization reaction, the aqueous layer was carefully collected. The suspension was purified by centrifugation using double-distilled water until the suspension reached a neutral pH value.

2.3 Preparation of GN/PANI/Au nanohybrids

The GN/PANI/Au nanohybrids were prepared through a simple one-step in situ reduction of Au^{3+} constructed on the GN/PANI nanocomposites. The HAuCl_4 (2.0 mL, 58.8 mM) and trisodium citrate (14.705 mg) were added to 20 mL GN/PANI (0.5 mg/mL) nanocomposites with stirring for 6 h followed by adding 0.1 M ice-cold NaBH_4 solution with stirring until the light-yellow solution turned to wine red, upon which it was centrifuged and washed with double-distilled water to obtain the GN/PANI/Au nanohybrids.

2.4 Materials Characterization

Transmission electron microscopy (TEM) and high resolution TEM (HRTEM) measurements were performed using a JEM-2100 transmission electron microscope (JEOL Ltd.). The TEM samples were prepared by dispensing a small amount of nanocomposites in doubly distilled water. Then, one drop of the suspension was dropped on 300 mesh copper TEM grids covered with thin amorphous carbon films.

The electrochemical measurements were carried out using a CHI 660E electrochemical analyser (Shanghai Chenhua Co.) with a standard three-electrode system composed of Ag/AgCl reference electrode, Pt wire counter-electrode, and the modified electrode as the working electrode. Prior to experiment, the glassy carbon electrode (GCE, 3 mm in diameter) was carefully polished with

alumina slurry (1.0, 0.3, and 0.05 μm) until a mirror like surface was achieved, then rinsed with distilled water followed by sonication in nitric acid (1:1), ethanol, and distilled water, and then dried in a stream of nitrogen gas. The 7 μL 0.8 mg/mL suspension was uniformly dropped on the pretreated GCE surface and dried at room temperature.

3. RESULT AND DISCUSSION

3.1 Characterization of nanohybrids

UV-vis absorption spectra was firstly supplied to characterize the synthesis of GN/PANI/Au nanohybrids. GN gives a maximum absorbance at $\lambda = 264$ nm (Fig. 1a), which is attributed to the $\pi\text{-}\pi^*$ transition in graphene sheets [14]. The spectra of the PANI contains two absorbance peaks at $\lambda = 330$ and 643 nm (Fig. 1b) ascribed to the $\pi\text{-}\pi^*$ transition of the benzenoid rings, and the π -polaron transition, respectively [19]. The absorption peak of GN is red shifted by 6 nm to $\lambda = 270$ nm in GN/PANI nanocomposites (Fig. 1c), which can be attributed to the $\pi\text{-}\pi$ interactions between PANI and GN molecules. The absorption spectrum of GN/PANI/Au nanohybrids shows a new broad absorbance peak at 560 nm compared with GN/PANI nanocomposites (Fig. 1d). The absorption peak of Au NPs at 560 nm was attributed to the surface plasmon resonance absorption of Au NPs [20, 21], suggesting the formation of Au NPs on the surface of GN/PANI nanocomposites.

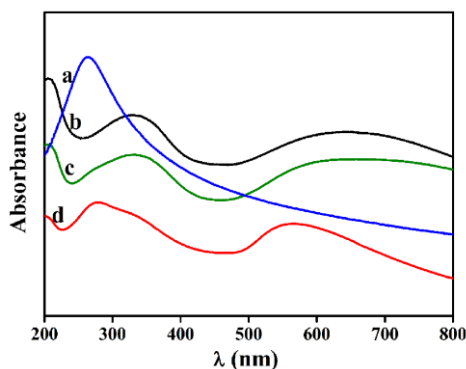


Figure 1. The UV/Vis spectra of (a) GN, (b) PANI, (c) GN/PANI and (d) GN/PANI/Au nanohybrids.

The morphology and structure of GN and GN/PANI nanocomposites were characterized by transmission electronic microscopy (TEM). The TEM image of GN showed clearly a transparent thin films with a wrinkled flake-like structure (Fig. 2A). After interfacial polymerization, the GN nanosheets were translucent without any aggregations, and PANI forms an ultrathin film and homogeneously coats the GN nanosheets (Fig. 2B). The results further prove that interfacial polymerization method is a very general route to create high-quality GN/PANI nanocomposites. In this method, the function groups of GN nanosheet provide nucleation sites for the growth and polymerization of PANI. The polymerization occurs at an aqueous/organic interface and terminates as

the GN/PANI nanocomposites diffuse into the top aqueous phase. Moreover, FeCl_3 as gentle oxidant has a decisive influence on the formation of a ultrathin PANI film coated onto the GN nanosheets. The interfacial polymerization method can effectively suppress secondary growth of polyaniline. Therefore PANI can be uniformly grown onto the surface of GN [18].

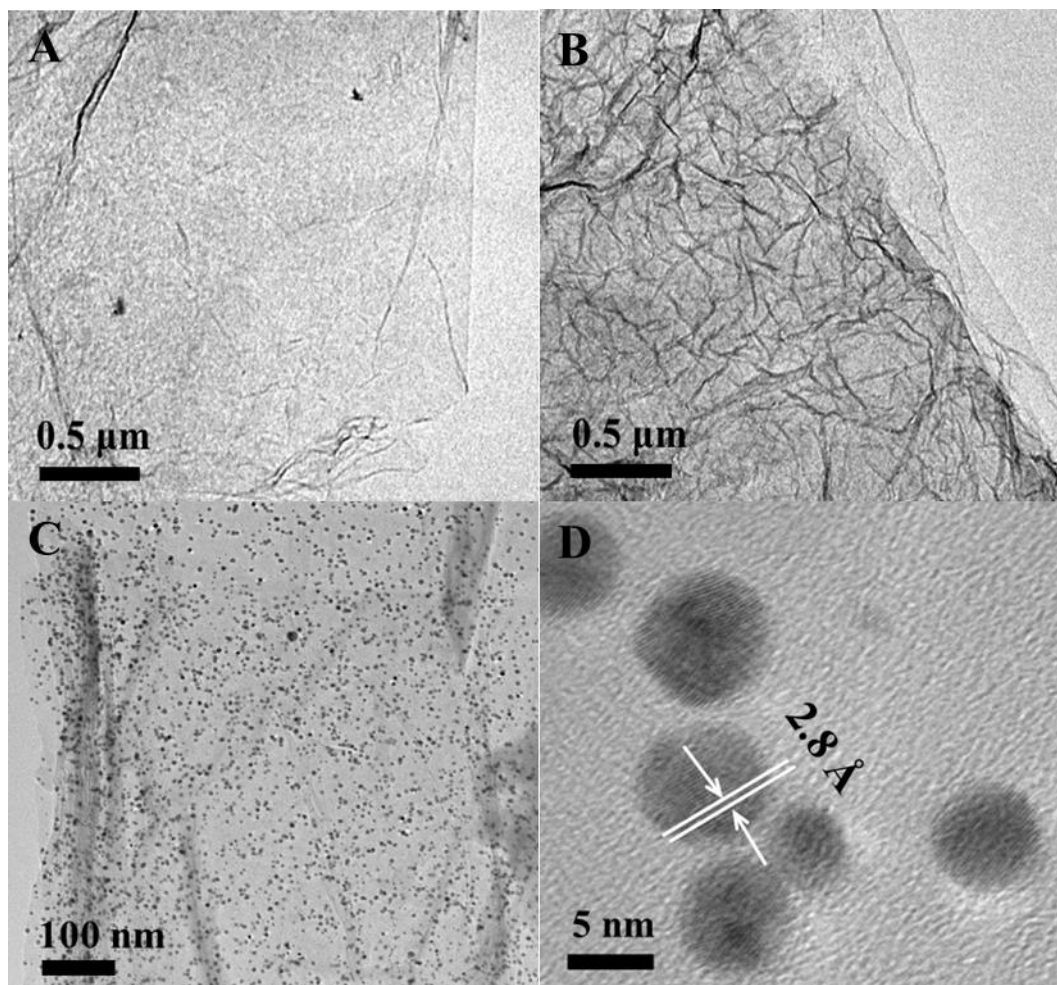


Figure 2. TEM images of GN (A), GN/PANI (B), GN/PANI/Au nanohybrids (C). HRTEM images of GN/PANI/Au nanohybrids (D).

PANI molecules have a great deal of functional groups and these groups can immobilize metallic nanoparticles in situ [22]. The formation of GN/PANI/Au nanohybrid was proven by TEM observation. As can be seen in Figure 2C, Au NPs are uniformly distributed on surface of GN/PANI. Additionally, we can't observe aggregated graphene and, that maybe due to the Au NPs decorated on the GN/PANI surfaces can act as “spacers” to prevent the GN/PANI from aggregating and restacking. The lattice structure of Au NPs can be observed clearly under the high magnification. Figure 2D reveals that the Au NPs with an average size about 5 ± 2.5 nm and the clear lattice fringes with the interfringe distance of 0.28 nm coincides with that of face centered cubic (fcc) Au (111).

The crystal structure of GN/PANI/Au nanohybrids was further supported by XRD patterns (Fig. 3). The reflection peaks of the GN/PANI/Au exhibited at 2θ of 38° , 44° , 65° , 78° and 82° are

consistent with the (111), (200), (220), (311), and (222). These results strongly indicate the existence of face-centered cubic Au NPs loaded on GN/PANI nanocomposites [23].

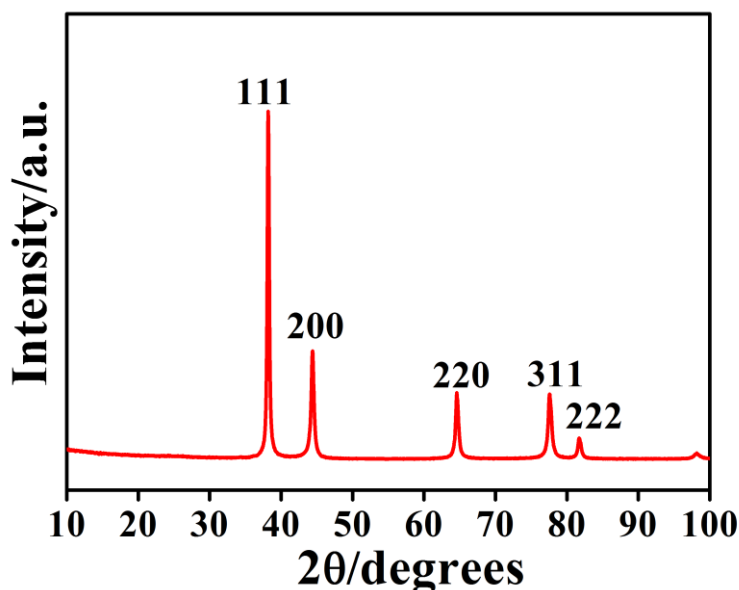


Figure 3. XRD patterns of GN/PANI/Au nanohybrids.

3.2 Electrochemical characterization of the modified electrodes

The charge transfer property of different types of electrodes were characterized by cyclic voltammograms (CVs). The cyclic voltammogram (CV) curve of the GN/GCE showed a pair of redox peaks with the potential difference (ΔE_p) as 88 mV (Fig.4, curve a). The GN/PANI/GCE also showed a pair of redox peaks and the peak currents increased and the potential difference became smaller (Fig.4, curve b) compared with GN modified GCE. While GN/PANI/Au nanohybrids modified GCE showed a pair of well-defined quasi-reversible redox peaks, the redox peak currents further increased and the ΔE_p further decreased (Fig.4, curve c), which could be attributed to the large surface area of the GN/PANI/Au nanohybrids and can accelerate the electron transfer of $\text{Fe}(\text{CN})_6^{3-/4-}$ [24].

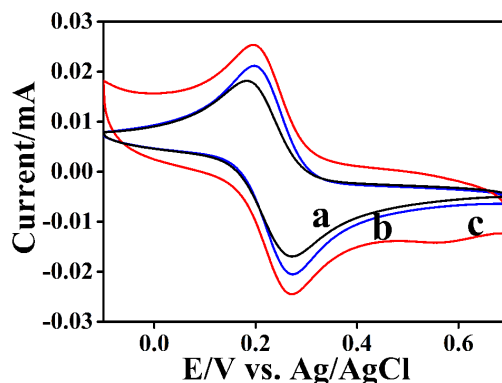


Figure 4. CVs of the GN/GCE (curve a), GN/PANI/GCE (curve b) and GN/PANI/Au/GCE (curve c) in 1.0 mM $\text{Fe}(\text{CN})_6^{3-/4-}$ solution containing 0.1 M KCl. Scan rate: 50 mV/s.

3.3 Electrochemical behaviors of AA, DA and UA

The individual electrochemical behaviors of AA, DA and UA at a bare GCE, GN/PANI/GCE and GN/PANI/Au/GCE were first investigated by CV (Fig. 5A). The concentrations of AA, DA, and UA are 1.39 mM, 1.81 mM, and 0.56 mM, respectively. At the bare GCE (curve a), only one anodic peak is obtained near 600 mV, and the peak potentials of DA, UA and AA are indistinguishable, indicating poor selectivity and sensitivity. And two anodic peaks are observed on GN/PANI/GCE near 439 mV and 682 mV (curve b), and the peak potentials of DA, UA and AA are indistinguishable. In contrast, three anodic peaks corresponding to AA, DA, and UA are observed on GN/PANI/Au/GCE (curve c). The peak currents are remarkably enhanced, the oxidation peak of AA, DA, and UA appear at about 131 mV, 408 mV, and 622 mV, respectively. The peak potential separations between AA and DA peak potentials is 277 mV, DA and UA is 214 mV, AA and UA is 491 mV. Which is larger than that obtained functionalized-graphene modified graphite electrode (199 mV for AA and DA, 164 mV for DA and UA, and 363 mV for AA and UA) [25] and ERGO/GCE (240 mV for AA and DA, 130 mV for DA and UA)[26]. Fig. 5B shows the DPV responses of AA, DA and UA at the GN/PANI/Au nanohybrids modified GCE. Three well defined oxidation peaks with larger peak separations to the oxidation of AA, DA and UA were observed at the GN/PANI/Au/GCE. The peak potentials at about 447 mV, 633 mV and 789 mV for AA, DA and UA, respectively. The DPV results show that GN/PANI/Au possesses good electrocatalytic activity can enhance the oxidation of AA, DA, and UA.

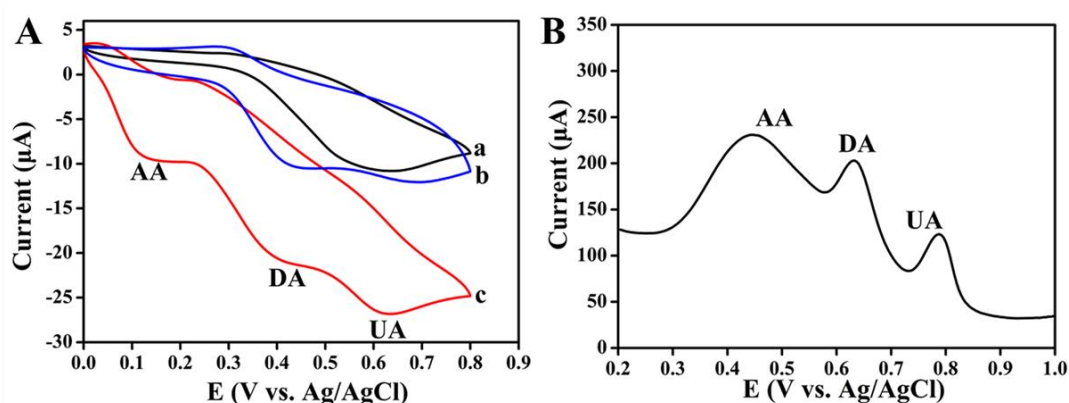


Figure 5. (A) CVs of the bare GCE (curve a), GN/PANI/GCE (curve b) and GN/PANI/Au/GCE (curve c) in 0.2 M PBS (pH 7.0) containing 1.39 mM AA, 1.81 mM DA and 0.56 mM UA; (B) DPV of AA, DA, and UA at the GN/PANI/Au/GCE, scan rates 50 mV/s.

3.4 Effect of scan rate

The kinetics of electrode reaction was investigated by exploring the scan rate dependence toward the anodic oxidation peak current of AA, DA, and UA. At the GN/PANI/Au/GCE (Fig. 6A and C), UA and AA show irreversible oxidation peaks at around 415 and 800 mV, respectively. And the oxidation peak potentials of AA and UA on the GN/PANI/Au/GCE underwent small positive shifts with increasing scan rate (10-100 mV/s). Fig.6B shows the CV curve for GN/PANI/Au/GCE in 0.2 M

PBS (pH 7.0) containing 0.86 mM DA at different scan rate. The oxidation and reduction peak current increased with increasing scan rates (10-100 mV/s). The peak currents of all three compounds linearly increase with the the square root of scan rate (inset plot of Fig. 6). This linearity suggests that electrochemical reactions of AA, DA and UA on the surface of GN/PANI/Au/GCE are diffusion controlled process. The linear regression equation of AA was $I_{pa}(\mu A)=0.3737+0.1568v^{1/2}$ $((mV s^{-1})^{1/2})$, $R=0.9984$), the linear regression equation of DA was $I_{pa}(\mu A)=0.126+0.0576v^{1/2}$ $((mV s^{-1})^{1/2})$, $R=0.9976$), and the linear regression equation of UA was $I_{pa}(\mu A)=0.224+0.1057v^{1/2}$ $((mV s^{-1})^{1/2})$, $R=0.9977$).

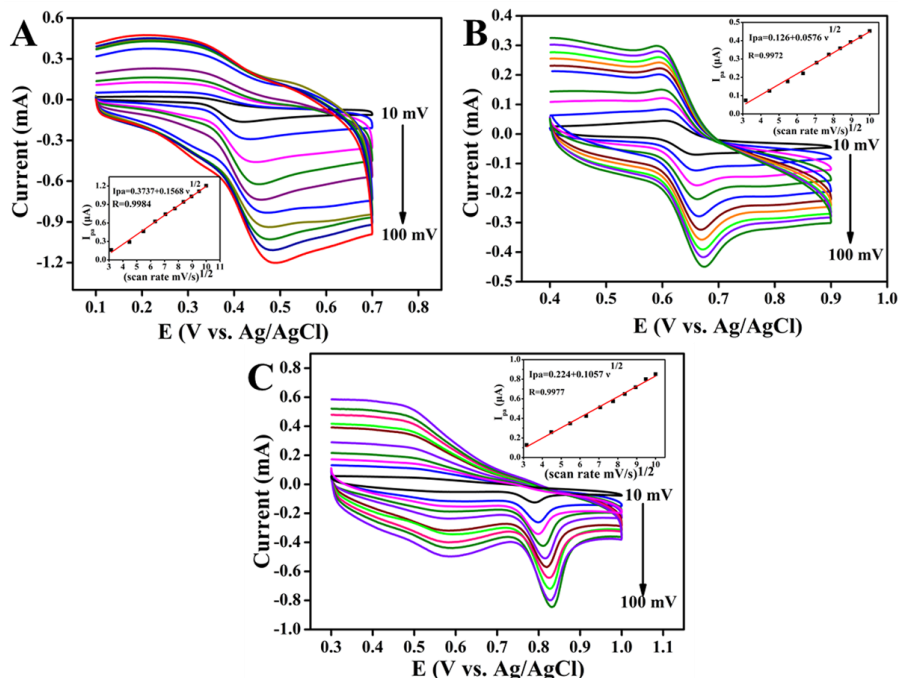


Figure 6. CVs of GN/PANI/Au/GCE in 0.2 M PBS (pH 7.0) respectively containing 2.86 mM AA (A), 0.86 mM DA (B), and 1.71 mM UA (C) with different scan rates (10, 20, 30, 40, 50, 60, 70, 80, 90, and 100 mV/s).

3.5 Simultaneous determination of AA, DA and UA on GN/PANI/Au/GCE

DPV was utilized to evaluate the selectivity and sensitivity of GN/PANI/Au hybrids for the simultaneous determination of AA, DA and UA. The detection of AA, DA and UA in their mixture solution were carried out when the concentration of one compound changed, whereas those of the other two compounds were keeping constant. As shown in Fig.7, the electrochemical response of target molecular increased linearly with the increase of concentration. The DPV peak currents of AA show a good linear relationship ($R=0.996$) with the concentration of AA from 1.55 to 33.22 mM in the presence of 0.28 mM DA and 0.71 mM UA. The results show that oxidation current increase linearly with the concentration of AA. The calibration curve for AA is displayed as $I_{pa}(\mu A)=152.1+4.37C_{AA}$ (mM) (Fig. 7 B). No obvious interference could be found for the determination of AA by the coexisting DA and UA. The limits of detection for AA is found to be 0.44 mM ($S/N=3$), with the linear

concentration ranges of 1.55-9.94 mM. And the linear concentration ranges is larger than the other [27, 28]. Fig. 7 C and D show the anodic peak current of DA increase linearly with the DA concentration increasing in the presence of 1.34 mM AA and 0.71 mM UA. The linear range of DA is from 0.07 to 5.24 mM. The regression equations were $I_{pa1}=142.27+76.49C_{DA}$ (μA , mM, $R=0.979$), $I_{pa2}=209.36+16.48C_{DA}$ (μA , mM, $R=0.992$). The limits of detection for DA is found to be 0.024 mM ($S/N=3$) with the linear concentration ranges of 0.07-1.05 and 1.47-5.24 mM. The limits of detection is lower than PASAB/GCE (0.046 mM.) [29]. No obvious interference could be found for the determination of DA by the coexisting AA and UA. Fig. 7E illustrates the DPV curves of UA in the presence of 1.34 mM AA and 0.14 mM DA, the anodic peak current increase linearly with increasing the concentration of UA from 0.14 to 6.02 mM. The regression equation is $I_{pa}=72.09+739.35C_{UA}$ (μA , mM, $R=0.983$) (Fig. 7F). The limits of detection for UA is found to be 0.047 mM ($S/N=3$) with the linear concentration ranges of 0.14-2.9 mM. The results show that interfering species was not significantly affected for detecting of target molecular. Table 1 summarizes the analytical performances of our fabricated GN/PANI/Au/GCE and the literature methods in terms of linearity and limits of detection.

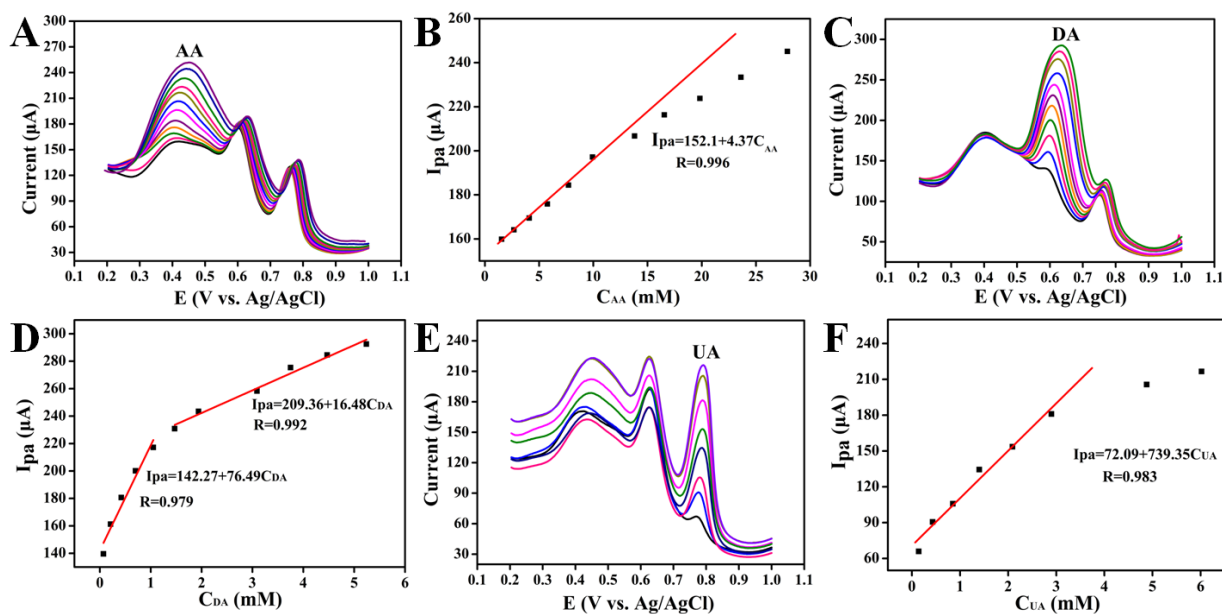


Figure 7. DPVs at the GN/PANI/Au/GCE in 0.2 M PBS (pH 7.0) containing ternary mixture of 0.28 mM DA, 0.71 mM UA and different concentrations of AA: 1.55, 2.68, 4.09, 5.77, 7.72, 9.94, 13.81, 16.55, 19.83, 23.62, 27.91, and 33.22 mM (A); the linear relationship between currents and AA concentration (B), containing 1.43 mM AA, 0.71 mM UA and different concentrations of DA: 0.07, 0.21, 0.42, 0.70, 1.05, 1.47, 1.94, 3.09, 3.75, 4.47, and 5.23 mM (C); the linear relationship between currents and DA concentration (D), containing 0.14 mM DA, 1.43 mM AA and different concentrations of UA: 0.14, 0.43, 0.85, 1.40, 2.09, 2.90, 4.88, and 6.02 mM (E), the linear relationship between currents and UA concentration (F).

Table 1. Comparison of analytical performance of GN/PANI/Au/GCE with other modified electrodes in the literature.

Electrode	Ascorbic acid (mM)		Dopamine (mM)		Uric acid (mM)		ref
	Linearity	LOD	linearity	LOD	Linearity	LOD	
MWNT-SiNW-AuNPs/GCE	1-5						[27]
PSS/SWNTs/GCE	1.0-0.1	0.05					[28]
PASAB/GCE	0.2-2.5	0.033	0.02-0.45	0.046			[29]
GN/PANI/Au/GCE	1.55-9.94	0.44	0.07-1.05 and 1.47-5.24	0.024	0.14-2.9	0.047	This work

3.6 Interference study

The influence of various substances on the determination of 2.0 mM AA, 1.0 mM DA, and 1.0 mM UA was studied by typical current-time responses. We found that 80-fold (vs. DA and UA) Na₂CO₃, NaNO₃, KCl, and NaCl, 40-fold (vs. AA) Na₂CO₃, NaNO₃, KCl, and NaCl not interfere with the determination (change in signal was less than 5%) (Fig. 8). The results strongly indicate that the as prepared GN/PANI/Au electrochemical sensor performs with high selectivity and little interference for determination of AA, DA and UA .

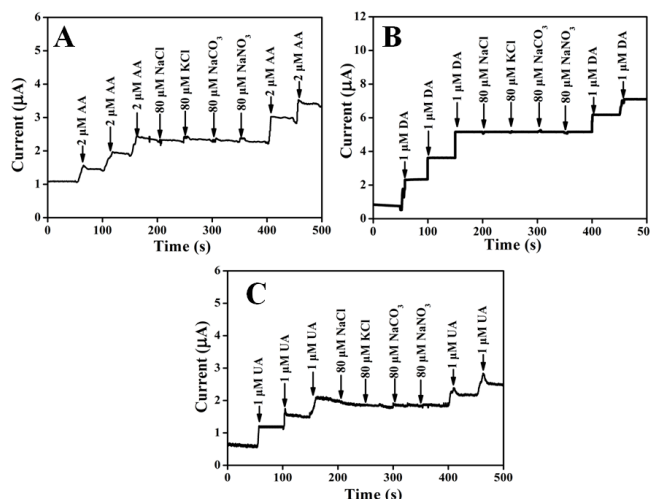


Figure 8. Amperometric responses of GN/PANI/Au/GCE upon successive addition of (A) 2 μM AA, (B) 1 μM DA, (C) 1 μM UA, and other chemicals to 0.2 M phosphate (pH 7.0). The applied potentials for AA, DA, and UA are 0.2, 0.5, and 0.6 V, respectively.

4. CONCLUSION

GN/PANI composites were prepared used liquid-liquid interface polymerization method, and then well-dispersed Au NPs supported on GN/PANI composites were obtained by a simple in situ reduction. As prepared GN/PANI/Au nanohybrids modified GCE was successfully constructed and used for determination of AA, DA and UA. The fabricated sensor show good catalytic activity and

selectivity toward AA, DA, and UA oxidation. This was attributed to the large surface areas, excellent catalytic activity and high conductivity of GN/PANI/Au nanohybrids.

ACKNOWLEDGEMENTS

This work was supported by the National Natural Science Foundation of China (No. 61361002), the National Natural Science Foundation of China (No. 21665008), Youth project of Yunnan Province (No 2014FD054), the key Project of Open Fund for Master Construction Disciplines of Yunnan Province (No. HXZ1304), the Scientific Research Fund Project of Honghe University (XJ14Z02).

References

1. Y. Y. Ling, Q. A. Huang, M. S. Zhu, D. X. Feng, X. Z. Li and Y. Wei, *J. Electroanal. Chem.*, 693(2013) 9.
2. J. Du, R. R. Yue, F. F. Ren, Z. Q. Yao, F. X. Jiang, P. Yang and Y. k. Du, *Biosens. Bioelectron.*, 53(2014) 220.
3. H. Manjunatha, D. H. Nagaraju and G. S. Suresh, *Electroanal*, 21(2009) 2198.
4. L. Q. Yang, N. Huang, Q. J. Lu, M. L. Liu, H. T. Li, Y. Y. Zhang and S. Z. Yao, *Anal. Chim. Acta*, 903(2016) 69.
5. W. H. Cai, J. W. Lai, T. Lai, H. T. Xie and J. S. Ye, *Sens. Actuators, B*, 224(2016) 225.
6. A. A. Abdelwahab and Y. B. Shimb, *Sens. Actuators, B*, 221(2015) 659.
7. Y. J. Yang, *Sens. Actuators, B*, 221(2015) 750.
8. M. M. Liu, R. Z. Zhang and W. Chen, *Chem. Rev.*, 114(2014) 5117.
9. M. D. Stoller, S. J. Park, Y. W. Zhu, J. H. An and R. S. Ruoff, *Nano Lett*, 8(2008) 3498.
10. D. C. Wei, Y. Q. Liu, Y. Wang, H. L. Zhang, L. P. Huang and G. Yu, *Nano Lett*, 9(2009) 1752.
11. U. Bogdanović, I. Pašti, G. Cirić-Marjanović, M. Mitrić, S. P. Ahrenkiel and V. Vodnik, *ACS Appl. Mater. Interfaces*, 7(2015) 28393.
12. F. Y. Kong, X. Zhu, M. T. Xu, J. J. Xu and H. Y. Chen, *Electrochim. Acta*, 56(2011) 9386.
13. W. S. Hummers Jr and R. E. Offeman, *J. Am. Chem. Soc.*, 80(1958) 1339.
14. D. Li, M. B. Mueller, S. Gilje, R. B. Kaner and G. G. Wallace, *Nat Nanotechnol*, 3(2008) 101.
15. H. J. Shin, K. K. Kim, A. Benayad, S. M. Yoon, H. K. Park, I. S. Jung, M. H. Jin, H. K. Jeong, J. M. Kim, J. Y. Choi and Y. H. Lee, *Adv Funct Mater*, 19(2009) 1987.
16. J. F. Shen, Y. Z. Hu, C. Li, C. Qin and M. X. Ye, *Small*, 5(2009) 82.
17. J. F. Shen, Y. Z. Hu, M. Shi, X. Lu, C. Qin, C. Li and M. X. Ye, *Chem. Mater.*, 21(2009) 3514.
18. J. D. Qiu, L. Shi, R. P. Liang, G. C. Wang and X. H. Xia, *Chem. Eur. J.*, 18(2012) 7950.
19. M. Zhao, X. M. Wu and C. X. Cai, *J Phys Chem C*, 113(2009) 4987.
20. S. J. Tan, M. J. Campolongo, D. Luo and W. Cheng, *Nat Nanotechnol.*, 6(2011) 268.
21. M. Iliut, C. Leordean, V. Canpean, C. M. Teodorescu and S. Astilean, *J. Mater. Chem. C*, 1(2013) 4094.
22. S. H. Xuan, Y. X. J. Wang, J. C. Yu and K. C. F. Leung, *Langmuir*, 25(2009) 11835.
23. Y. J. Hu, J. Jin, P. Wu, H. Zhang and C. X. Cai, *Electrochim Acta*, 56(2010) 491.
24. L. M. Lu, H. B. Li, F. L. Qu, X. B. Zhang, G. L. Shen and R. Q. Yu, *Biosens. Bioelectron.*, 26(2011) 3500.
25. Malledevaru Mallesh, Revanasiddappa Manjunatha, C. Nethravathi, Gurukar Shivappa Suresh, Michael Rajamathi, Jose Savio Melo and T. V. Venkatesha, *Bioelectrochemistry*, 81(2011) 104.
26. L. Yang, D. Liu, J. S. Huang and T. Y. You, *Sens. Actuators, B*, 193(2014) 166.
27. D. Ragupathy, A. I. Gopalan and K. P. Lee, *Sens. Actuators B*, 143 (2010) 696.
28. Y. Pan, I. P. Zhang, K. Y. Zhang, H. Y. MA and Y. Z. Zhang, *Journal of Anhui Normal University*, 30(2007) 575.

29. W. J. Zhao, W. J. Sun, J. L. Gao and Q. F. Weng, *Guangzhou Chemical Industry*, 39(2011) 119.

© 2017 The Authors. Published by ESG (www.electrochemsci.org). This article is an open access article distributed under the terms and conditions of the Creative Commons Attribution license (<http://creativecommons.org/licenses/by/4.0/>).